第35卷第5期
2016年10月

红外与毫米波学报
J. Infrared Millim. Waves

Vol. 35, No. 5
October, 2016

文章编号：1001－9014(2016)05－0538－05

DOI:10.11972/j.issn.1001－9014.2016.05.006

Numerical study of a dual-band metamaterial absorber in near infrared region based on cavity and electrical resonances

LI Xing-Wei[1*], BAI Shen-Jian[1], SUN Ji-Xiang[2]

(1. College of Mechatronic Engineering and Automation, National University of Defense Technology, ChangSha 410073, China;
2. College of Electronic Science and Engineering, National University of Defense Technology, ChangSha 410073, China)

Abstract: In this paper, we present the design, numerical simulations and analysis of a metamaterial absorber with two broad and flat absorption bands, including a cavity resonance band and an electrical resonance band. The electrical resonance band reveals a blue-shift with the width of cavity (d) or spacer thickness (H) increasing, while the cavity resonance band exhibits a red-shift with d or H increasing. Furthermore, electrical and cavity resonance bands can be coupled together at the same resonance wavelength to realize a single absorption band through optimizing the structure design. Finally, the effects of the variation of angles of incidence on electrical and cavity resonance bands were simulated. This method of utilizing different resonant modes for absorption bands at different wavelengths offers a simple approach to modulate dual absorption bands to single absorption band.

Key words: metamaterial, absorber, resonance
PACS: 41.20.Jb, 78.20.Cj, 73.20.Mf

数值研究一种基于腔共振和电共振的近红外双频段超材料吸收器

李兴玮[1*]，白圣建[1]，孙即祥[2]
(1. 国防科学技术大学 机电工程与自动化学院，湖南 长沙 410073；
2. 国防科学技术大学 电子科学与工程学院，湖南，长沙 410073)

摘要：设计，数值模拟和讨论了一种具有两个宽带和扁平的吸收带的超材料吸收器，其中一个是腔共振吸收带，另一个是电共振吸收带.电共振的吸收带由于空腔尺寸(d)或者介质层厚度(H)的增加而蓝移，而腔共振吸收带则表现出红移的现象.同时，电共振和腔共振吸收带可以通过优化吸收器的结构设计耦合为一个吸收带.最后，数值模拟研究了入射角度的改变对电共振和腔共振吸收带的影响.利用不同波段的共振模式形成不同吸收带的方式提供了将双吸收带调制为单吸收带的可能性.

关 键 词：超材料；吸收器；共振

中图分类号：O431　　**文献标识码**：A

Introduction

Metamaterial is an artificial array of subwavelength structure that can be designed and produced to achieve non natural material properties, such as negative refractive index, negative permittivity, etc. Since Smith et al experimentally demonstrated the negative refractive index, metamaterials have been studied on different designs, and manufactured in a wide range of applications, such as cloak, imaging, emitters, and perfect electromagnetic absorbers[1-7]. Metamaterial absorber has become a popular topic since it was firstly reported by Landy *et al.* [8] in 2008. Metamaterial absorbers have displayed near perfect or perfect absorption in targeted frequency region, such as microwave, visible, terahertz (THz) and infrared (IR) frequencies[8-12]. To date, metamaterial absorbers have been widely studied in microwave and THz region compared with IR and visible frequency region, because their large feature sizes of single unit cell that are easier to be designed and fabrica-

Received date: 2015-10-17, **revised date**: 2016-05-03　　**收稿日期**：2015-10-17，**修回日期**：2016-05-03
Foundation items: Supported by The Study on the Hardware-In-The-Loop Simulation Technology of Strapdown Seeker (201003750)
Biography: LI Xing-Wei (1969-), male, Ph. D., associate professor. Research area involves system simulation, navigation, guidance and control, image processing, Circuits and Systems.
* **Corresponding author**: E-mail: simu_lxw@nudt.edu.cn

ted. Even though, IR perfect metamaterial absorbers are also expected to achieve broad band in recently, owing to the increasing demands in the applications of IR metamaterial absorbers, such as solar cells, IR detectors, chemical sensing[13-15]. For dual- and multi-band IR perfect metamaterial absorbers, most of the structure design strategies employ the electrical resonance or plasmonic in the top metal layer, either through adopting single structured pattern layer with respect to the polarization, or through utilizing two or more metal and dielectric layers in a single unit cell[16-19]. First of all, the metamaterial absorbers that were reported above are generally difficult to be designed and fabricated, due to that they consist of multiple layers or adopt exotic materials. Secondly, simpler absorbers which consist of single metamaterial pattern layer with split symmetry are always polarization sensitive, which hinds their practical applications. Most of structures of the above IR metamaterial absorbers adopt either silver or gold as the material of top and bottom structural layers. Meanwhile, self-assembly, electron beam lithography, or focused ion beam are usually used for fabrication process.

In this paper, we designed and simulated a dual-band metamaterial absorber with a modified fishnet structure. The modified fishnet structure consists of a single top metal unit cell layer and a bottom reflector metal layer separated by a single spacer dielectric layer. Molybdenum (Mo) is used as the top and bottom metal layers, while Calcium carbonate (CaCO3) is used as the spacer dielectric layer. Two absorption bands are achieved corresponding to electrical and cavity resonance modes at different wavelengths, respectively. The cavity resonance mode is achieved from the dielectric layer cavity formed between the top and bottom metal layers, while the electrical resonance mode is obtained due to the coupling of modes excitation in the top and bottom metal layers. The dual-band metamaterial absorber can be modulated to be a single band absorber by optimizing geometric parameters to excite these resonance modes at the same wavelength.

1　Unit cell design and its absorption spectrum

Figure 1 shows the geometry of the designed absorber structure which consists of top silver layer, SiO_2 spacer and bottom Mo layer. All dimensional parameters of the compound structure are as following: $H = 345$ nm, $P = 3\ 500$ nm, $d = 2\ 500$ nm, $w = 260$ nm, $s = 215$ nm. The Mo ground plane is thick enough that the designed structure does not allow any electromagnetic transmit, which leads to the transmission $T(\lambda)$ very close to zero. The absorption could be calculated as $A(\lambda) = 1 - R(\lambda)$, where $A(\lambda)$ is the wavelength-dependent absorption, and $R(\lambda)$ is the wavelength-dependent reflection. Ansofts HFSS 13.0 was applied to investigate the relationship between the resonance wavelength and the intensity of current distributions. The Mo layer follows the Drude model:

$$\varepsilon(\omega) = 1 - \frac{\omega_p^2}{\omega^2 - i\omega\gamma_D} \quad . \quad (1)$$

Here, $\omega_p = 1.37 \times 10^{16}\ s^{-1}$ is the plasma frequency, $\gamma_D = 9 \times 10^{13}\ s^{-1}$ is the collision frequency[20]. The complex permittivity of the lossless $CaCO_3$ layer is set to 2.102 5[21]. In our simulation, two ideal magnetic conductor planes and two ideal electric conductor planes were applied on the boundary normal to the x axis and y axis[22]. The simulated absorption spectra for the dual-band metamaterial absorber are shown in Fig. 1(c). In Fig 1(c), the absorption band width is defined as: $\Delta\lambda = \lambda_{high} - \lambda_{out}$, the range between λ_{high} (the higher-wavelength point at which 95% energy is absorbed by the designed structure) and λ_{out} (the lower-wavelength point at which 95% energy is absorbed by the designed structure). A low-wavelength absorption band (the bandwidth is $\Delta\lambda_{low} = 0.12$ μm, the average absorption magnitude is 96.1%) and a high-wavelength absorption band (the bandwidth is $\Delta\lambda_{high} = 0.12$ μm, the average absorption magnitude is 95.4%) can be observed, as shown in Fig 1(c).

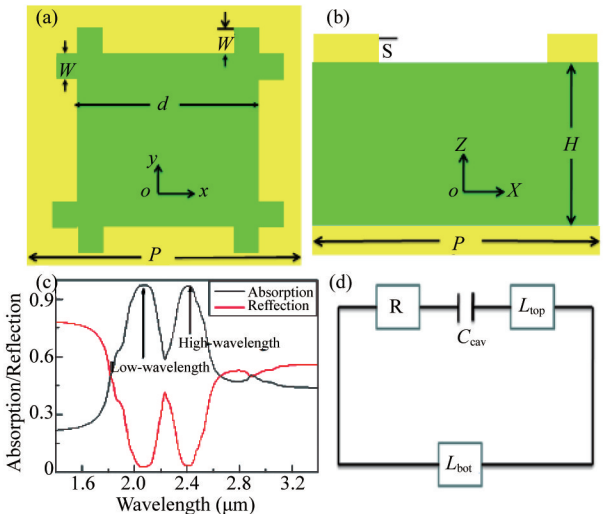

Fig. 1　(a) Top view of a unit cell. (b) Side view of a unit cell on the xoz plane. The yellow part is Mo layer, the green part is $CaCO_3$ layer, (c) Simulated absorption and reflection spectra. (d) Equivalent *LC* circuit for the designed metamaterial absorber at electrical resonance

图 1　(a)结构单元的俯视图,(b)结构单元的侧视图在 xoz 平面;其中黄色部分是 Mo 层,绿色部分是介质层,(c)仿真的吸收率和反射率谱,(d)与设计的超材料吸收器的电共振等价的 *LC* 电路

In order to understand the mechanisms behind these absorption bands, patterns of the current distributions on the xoz plane were investigated, which would offer an insight into the influence of electromagnetic responses on absorption bands. The simulated current density distributions inside of two absorption bands[23] are shown in Fig. 2. In the low-wavelength band, a resonant wavelength was selected, such as $\lambda = 2.1$ μm, a reverse current can be observed in the top and bottom Mo layers obviously, which indicates that the low-wavelength band is excited by the cavity resonance[24], as shown in Fig. 2(a-b). In the high-wavelength band, another resonant wavelength was also selected, such as $\lambda = 2.45$ μm, the majority

surface current is concentrated on the top Mo layer and a weaker surface current is concentrated on the bottom Mo layer, which indicates that the high-wavelength absorption band is excited through the electrical resonance between the top and bottom Mo layers[24], as shown in Fig. 2 (c-d). These two resonance modes are the mechanisms which lead to the dual absorption bands in Fig. 1 (c). In the following sections, the two absorption bands are named as the "cavity resonance band" and the "electrical resonance band" for convenience.

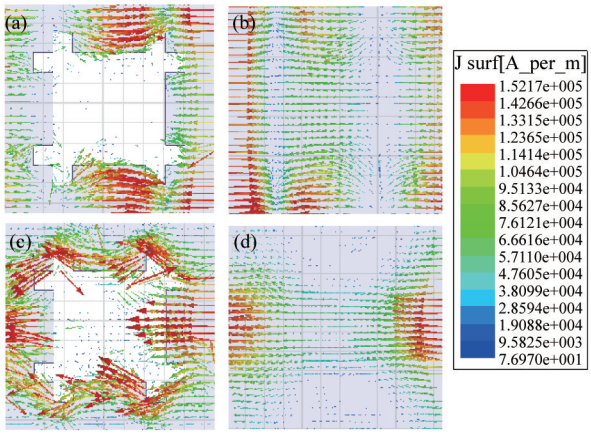

Fig. 2 Cavity resonance, $\lambda = 2.1$ μm: (a) surface current distribution in the top Mo layer, (b) simulated surface current distribution in the bottom Mo layer. Electrical resonance, $\lambda = 2.45$ μm: (c) simulated surface current distribution in the top Mo layer, (d) simulated surface current distribution in the bottom Mo layer

图2 在 $\lambda = 2.1$ μm 的腔共振:(a)在顶部 Mo 层的表面电流分布,(b)在底部 Mo 层的表面电流分布. 在 $\lambda = 2.45$ μm 的电共振:(c)在顶部 Mo 层的表面电流分布,(d)在底部 Mo 层的表面电流分布

2 Study on geometrical variation

To get inside into dual absorption bands because of the electrical resonance and cavity resonance, two sets of simulations were carried out-one varying the width of cavity (d) at fixed thickness (H) of the dielectric layer, while other varying H at fixed d.

2.1 Effect of the width of cavity (d)

To study the effect of the variation in d on these absorption bands, the first set of simulations was carried out: d is increased from $d = 2\,500$ nm to $d = 2\,620$ nm, while other geometrical parameters unchanged. Fig. 3 shows the simulated absorption spectra. It reveals that the central wavelength of the electrical resonance band exhibits a shift from $\lambda = 2.45$ μm ($d = 2\,500$ nm) to, $\lambda = 2.37$ μm ($d = 2\,620$ nm). However, the band width of the electrical resonance band increased slowly. This is due to that the intensity of the coupling and interaction of electrical resonance modes between the top and bottom Mo layers are almost unchanged, which implies that the intensity of current is almost unchanged. A lumped equivalent LC circuit of the designed unit cell structure was carried out to exploit the effect of d on the central wavelength of the electrical resonant band, as shown in Fig. 1 (d). The resonant wavelength of this LC circuit can be described as follows[25-27]:

$$\lambda_o \approx 2\pi C_o \sqrt{C_{cav}(2L_{top} + L_{bot})} \quad . \quad (2)$$

Here, λ_o is the resonance wavelength, C_o is the speed of light in vacuum, C_{cav} is the equivalent capacitance that is between the two opposite edges of the top structured Mo layer, L_{top} is the inductance due to the structured Mo layer, L_{bot} is the inductance due to bottom Mo layer. With d increasing, the value of C_{cav} is reduced, which leads to the reduction of λ_o according to Eq. (2) and shift of the electrical resonant band to lower wavelength, as shown in Fig. 3 (a-c). At the same time, the cavity resonance shows a red-shift with d increasing. Moreover, the band width is increased from 0.12 μm to 0.28 μm with d increase from C to $d = 2\,620$ nm. However, the band width is reduced to 0.08 μm when $d = 2\,620$ nm. The maximum absorption band of the cavity resonance is owing to that d primarily defines the surface impedance matching condition of the designed structure. So the increase in d would lead to a high impedance match between the top Mo layer and air interface, which results in the reduction of the reflection at the air-spacer interface with the top Mo layer and hence increasing the absorption at the resonant wavelength. When $d = 2\,590$ nm, the perfect impedance matching condition is reached[9] and the maximum absorption band is obtained. When $d = 2\,620$ nm, the cavity resonant band shrinks obviously due to that the impedance matching condition is destroyed. Moreover, the cavity and electrical resonant bands becomes close to each other when d is increased from $d = 2\,500$ nm to $d = 2\,590$ nm, which leads to mergence of the cavity and electrical resonant bands into a single absorption band ($d = 2\,590$ nm), as shown in Fig. 3 (d). This implies that the proposed dual-band metamaterial absorber can be modulated to be a single band absorber by optimized design of impedance matched conditions.

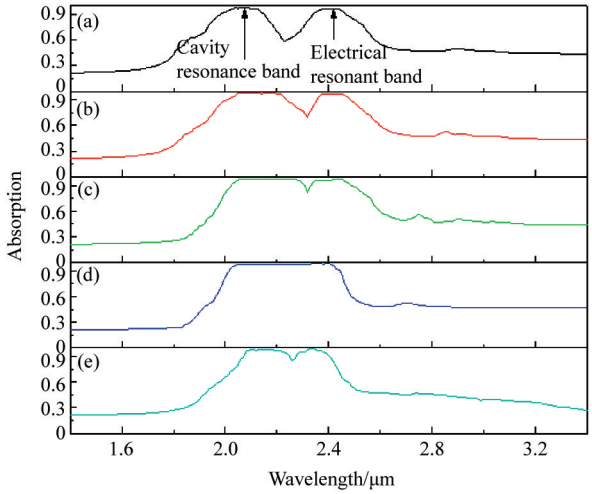

Fig. 3 Simulated absorption spectra of the designed metamaterial absorber with different samples: (a) $d = 2\,500$ nm, (b) $d = 2\,530$ nm, (c) $d = 2\,560$ nm, (d) $d = 2\,590$ nm, (e) $d = 2\,620$ nm

图3 不同的超材料吸收器的仿真吸收谱:(a) $d = 2\,500$ nm, (b) $d = 2\,530$ nm, (c) $d = 2\,560$ nm, (d) $d = 2\,590$ nm, (e) $d = 2\,620$ nm

2.2 Effect of spacer thickness (H)

The second set of simulations was carried out: varying H, while other structural parameters fixed. H is increased from $H = 345$ nm to $H = 435$ nm, as shown in Fig. 4. On the one hand, the electrical resonant band shows a blue-shift due to that H is increased and the band width is increased from 0.1 μm ($H = 345$ nm) to 0.22 μm ($H = 435$ nm). The increase of the electrical resonant band can be understood by Eq. (2). This is mainly owing to that the strength of the current in the bottom Mo layer is reduced with the increase of the dielectric layer thickness, which leads to the effective inductance in the bottom Mo layer reduce and the absorption band blue-shift. Thus, the intensity of coupling and interaction of electrical resonance modes between top and bottom Mo layers is reduced[28]. On the other hand, the cavity resonant band shows a red-shift with H increasing. The cavity resonant band width shows a slow increase due to the dielectric loss with H increasing[9]. It is interesting that the electrical resonant band and cavity resonant band merger into one single band as well with H increasing, as shown in Fig. 4(d).

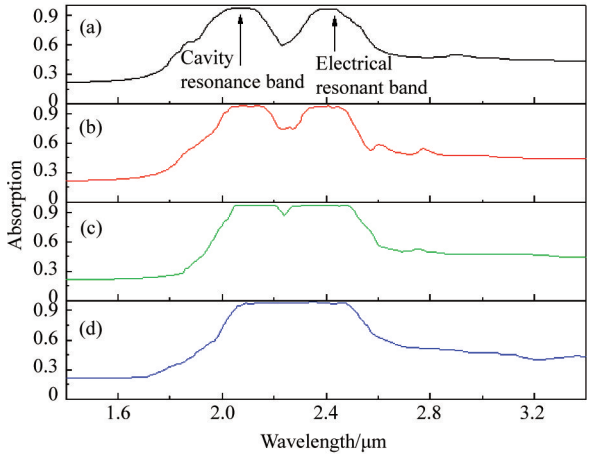

Fig. 4　Simulated absorption spectra of the metamaterial absorber with different spacer thickness: (a) $H = 345$ nm, (b) $H = 375$ nm, (c) $H = 405$ nm, (d) $H = 435$ nm

图 4 不同中间层厚度的超材料吸收器仿真吸收谱: (a) $H = 345$ nm, (b) $H = 375$ nm, (c) $H = 405$ nm, (d) $H = 435$ nm

To thoroughly study the designed structure, the effects of the variation of angles of incidence was simulated finally. Figure 5 shows the absorption spectra with normal, 15°, 30° and 45° angles. It can be found that both the average absorptions of the cavity and electrical resonant bands reach 85% when the angle of incidence is larger than 30°. However, the average absorption is reduced to 72% when the angle of incidence is 45°. It can be found that the bandwidths of cavity resonance band and electrical resonant band are reduced with the increase of the angle of incidence. However, the resonant wavelengths of these resonant absorption bands are almost unchanged, which is similar to the proposed work in the TE case[17]. It should be indicated that the designed structure in this paper consists a rotational symmetric pattern. Therefore, the performance of the absorption spectra of the designed structure is insensitive to the polarization of the incident waves, which indicates a superiority of the designed structure in the real application.

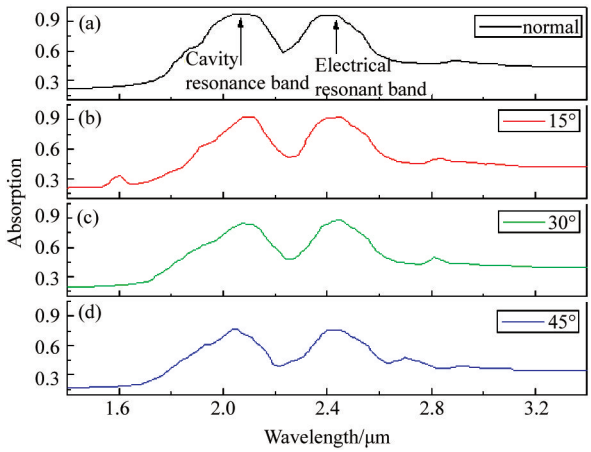

Fig. 5　Absorption spectra of the designed structure with different angles of incidence

图 5　不同入射角条件下的超材料吸收起的仿真吸收谱

3 Conclusion

In this paper, we present the simulations and analysis of the dual band metamaterial absorber. The low-wavelength absorption band is excited by the cavity resonance, while the high-wavelength absorption band is mainly due to the coupling and interaction of electrical resonance between the top Mo structured layer and bottom Mo layer. The absorption band width can be modulated through increasing d or H. On the one hand, the electrical resonant band shifts to lower wavelength due to that the value of C_{cav} is reduced with d increasing, while the cavity resonance band shifts to higher wavelength because of the higher impedance matched. On the other hand, the electrical resonant band demonstrates a shift to lower wavelength and increase of the band width owing to that the effective inductance in the bottom Mo layers is reduced, while the cavity resonant band shows a red-shift and the band width is increased due to the dielectric loss. Moreover, these resonant bands could be engineered to merge into a single absorption band by optimizing the structure parameters (d or H).

Acknowledgment

This research is financially supported by the study on the Hardware-In-The-Loop Simulation Technology of Strapdown Seeker (201003750)

References

[1] Schurig D, Mock J J, Justice B J, *et al*. Metamaterial electromagnetic cloak at microwave frequencies [J]. *Science*, 2006, **314**: 977-980.

[2] Liu N, Mesch M, Weiss T, *et al*. Infrared perfect absorber and its application as plasmonic sensor [J]. *Nano Lett*, 2010, **10**:2342-2348.

[3] Liu X, Tyler T, Starr T, *et al*. Taming the blackbody with infrared metamaterials as selective thermal emitters [J]. *Phys. Rev. Lett*, 2011, **107**: 045901-045904.

(下转第 591 页)

discoloration process for Gingko Biloba Metasequoia Glyptostroboides based on GIS in Sichuan Basin[D]. Chengdu: Sichuan Aricultural University. (付静静. 基于 gis 的四川盆地秋季红叶指数与银杏、水杉秋叶变色过程分析. 四川农业大学),2012.

[22] MALTHUS T J, MADERIA A C. High resolution spectrordiometry: spectral reflectance of field bean leaves infected by Botrytis Fabae[J]. *Remote Sensing of Environment*, 1993, **45**:107 - 116.

(上接 541 页)

[4] Hao J, Zhou L, Qiu M, Nearly total absorption of light and heat generation by plasmonic metamaterials [J]. *Phys. Rev. B*, 2011, **83**:165107 - 165119.

[5] Watts C M, Liu X, Padilla W J, Metamaterial electromagnetic wave absorbers [J]. *Adv. Mater.* 2012, **24**:OP98 - OP120.

[6] Wang Y T, Cheng B H, Ho Y Z, *et al*. Gain-assisted hybrid-superlens hyperlens for nano imaging [J]. *Opt. Express*, 2012, **20**: 22953 - 22960.

[7] Cheng B H, Lan Y C, Tsai D P, Breaking optical diffraction limitation using optical hybrid-super-hyperlens with radially polarized light [J]. *Opt. Express*, 2013, **21**:14898 - 14906.

[8] Muskens O L, Diedenhofen S L, Weert M H M, *et al*. Epitaxial growth of aligned semiconductor nanowire metamaterials for photonic applications [J]. *Adv. Funct. Mater*, 2008, **18**:1039 - 1046.

[9] Landy N I, Sajuyigbe S, Mock J J, *et al*. Perfect metamaterial absorber [J]. *Phys. Rev. Lett*, 2008, **100**:207402 - 207405.

[10] Wen Q Y, Zhang H W, Xie Y S, *et al*. Dual band terahertz metamaterial absorber: Design, fabrication, and characterization [J]. *Appl. Phys. Lett.* 2009, **95**:241111 - 241113.

[11] Hao J, Wang J, Liu X, *et al*. High performance optical absorber based on a plasmonic metamaterial [J]. *Appl. Phys. Lett.* 2010, **96**:251104 - 251106.

[12] Zhang N, Zhou P, Cheng D, *et al*. Dual-band absorption of mid-infrared metamaterial absorber based on distinct dielectric spacer layers [J]. *Opt. Lett.* 2013, **38**:1125 - 1127.

[13] Niesler F B P, Gansel J K, Fischbach S, *et al*. Metamaterial metal-based bolometers [J]. *Appl. Phys. Lett.* 2012, **100**: 203508 - 203511.

[14] Jaruwongrungsee K, Withayachumnankul W, Wisitsoraat A, *et al*. Metamaterial-inspired microfluidicbased sensor for chemical discrimination [J]. IEEE Sensors, 2012, **21**:01 - 04.

[15] Wang Y, Sun T, Paudel T, *et al*. Metamaterial plasmonic absorber structure for high efficiency amorphous silicon solar cells [J]. *Nano Lett.* 2012, **12**:440 - 445.

[16] Cheng D, Xie T, Zhang H, *et al*. Pantoscopic and polarization-insensitive perfect absorbers in the middle infrared spectrum [J]. *J. Opt. Soc. Am. B*, 2012, **29**:1503 - 1510.

[17] Lee H M, Wu J C. A wide-angle dual-band infrared perfect absorber based on metal-dielectric-metal split square-ring and square array [J]. *J. Phys. D: Appl. Phys.* 2012, **45**:205101 - 205106.

[18] Hendrickson J, Guo J, Zhang B, *et al*. Wideband perfect light absorber at midwave infrared using multiplexed metal structures [J]. *Opt. Lett.* 2012, **37**:371 - 373.

[19] Chen K, Adato R, Altug H, Dual-band perfect absorber for multispectral plasmon-enhanced infrared spectroscopy [J]. ACS Nano, 2012, **6**:7998 - 8006.

[20] Zhang S, Fan W J, Paniou N C, *et al*. Experimental Demonstration of Near-infrared Negative-Index Metamaterials [J], *Phys. Rev. Lett.* 2005. **95**:137404 - 137407.

[21] Kischkat J, Peters S, Gruska B, *et al*. Mid-infrared optical properties of thin films of aluminum oxide, titanium dioxide, silicon dioxide, aluminum nitride, and silicon nitride [J]. *Appl. Opt.* 2012, **51**:6789 - 6798.

[22] Smith D R, Schult S, Markos P, *et al*. Determination of effective permittivity and permeability of metamaterials from reflection andtrans- mission coefficients [J], P*hys. Rev. B*, 2002, **65**: 195104 - 195108.

[23] Ho C P, Pitchappa P, Kropelnicki P, *et al*. Development of polycrystalline silicon based photonic crystal membrane for mid-infrared applications [J]. *IEEE J. Sel. Top. Quantum Electron.* 2014, **20**: 4900107 - 4900113.

[24] Pitchappa P, Ho C P, Kropelnicki P, *et al*. Dual band complementary metamaterial absorber in near infrared region [J], *Journal of Applied Physics*, 2014, **115**:193109 - 193115.

[25] Zhou J, Economon E N, Koschny T, *et al*. Unifying approach to left-handed material design [J]. *Opt. Lett.* 2006, **31**:3620 - 3622.

[26] Pang Y, Cheng H, Zhou Y, *et al*. Analysis and design of wirebased metamaterial absorbers using equivalent circuit approach [J]. *J. Appl. Phys.* 2013, **113**:114902 - 114908.

[27] Zhou J, Koschny T, Soukoulis C M, An efficient way to reduce losses of left-handed metamaterials [J]. *Opt. Express*, 2008, **16**: 11147 - 11152.

[28] Hu C, Zhao Z, Chen X, *et al*. Realizing near-perfect absorption at visible frequencies [J]. *Opt. Express*. 2009, **17**:11039 - 11044.